KSCE Journal of Civil Engineering (2019) 23(7):3030-3040

DOI 10.1007/s12205-019-1912-2

Structural Engineering

pISSN 1226-7988, eISSN 1976-3808
www.springer.com/12205

Development of Virtual Load Rating Method for Taxiway Bridge under Aircraft Taxiing

Qian Dong*, Jianhua Wang, Xianmin Zhang***, Hao Wang****, and Xisha Jin*****

Received September 27, 2018/Accepted March 25, 2019/Published Online May 10, 2019

Abstract

This paper presents finite element model (FEM) based virtual load rating method for accurately and efficiently evaluating the bearing capacity of taxiway bridge in the field under aircraft taxiing. A dynamic load coefficient of aircraft loading was first developed considering deck pavement roughness and aircraft lift force. The in situ responses of taxiway bridges under 10 aircraft were collected using instrumentation system with acceleration sensor, strain sensor, and inclinometer. The modal frequency, strain influence lines, and deflections of taxiway bridge were obtained from FE analysis and in situ test. An optimization objective function in terms of fundamental frequency and strain influence lines was formulated to ensure convergence and effectiveness in the model updating process, wherein the bending stiffness, density and boundary conditions of the structures are selected as the design variables. The weighted-average method of model updating parameters was proposed considering the differences in the obtained parameters under different loading conditions. The analysis results of updated FE model were validated using static loading test conducted on taxiway bridge. Finally, the proposed virtual load rating method was applied to Taxiway Bridge V in Guangzhou Baiyun International Airport (CAN).

Keywords: *aircraft operation, finite element updating, strain influence lines, taxiway bridge, vibration mode*

1. Introduction

The rapid development of civil aviation is driving the increased traffic in major hub airports. Taxiway bridges and runway bridges were used to solve the conflict between airport design and geographical restrictions. For example, in Beijing Capital International Airport (PEK), Frankfurt am Main International Airport (FRA) (Stephan *et al.*, 2012), and Malpensa International Airport (MXP) (Malerba and Comaita, 2011), taxiway bridge is an important component of airfield facility. The fifth runway at Hartsfield Jackson Atlanta International Airport (ATL) is a long taxiway bridge with design load of 590 tons crossing a 10-lane highway. Moreover, the runway at Madeira Airport (FNC) is composed of a 914-m-long bridge and common runway because of geographical factors. The width of this runway bridge is more than 590 ft (about 180 m), and it can carry the weight of Boeing 747 and commuter jets. These bridges are required to have enough bearing capacity under heavy loading of large aircrafts in the service life. Therefore, it is needed to assess the bearing capacity of taxiway or runway bridges in the airfield accurately and efficiently. Currently, there is no standard national or international method for evaluating the bearing capacity of taxiway bridge. In China, such evaluations are conducted using the same test methods as for ordinary highway bridges, namely, static-load test method which involves closing the airport for 2 – 3 days until the work is finished. However, the airports with taxiway bridges are usually among the largest and busiest airports, suspending aircraft traffic involves enormous economic and social impacts. In addition, a taxiway bridge has its own characteristics that make it distinct from a highway bridge. First, the loading characteristic of taxiway bridges is different from those of highway bridges. The design load on taxiway bridge is considered to be the full weight of the largest aircraft during taxiing. Hence, the load on taxiway bridge is 8 – 30 times greater than the standard vehicle load but distributed in the space occupied by only two or three standard vehicles. This is one big difference between the loads acting on a highway bridge and a taxiway bridge. Second, the width–span ratio of a taxiway bridge is larger than that of a highway bridge. The Civil Aviation Administration of China's "Technical standards for airfield area of civil airports" (MH/T 5001-2013, 2013) mandates that taxiway bridge width should be no narrower than

*Ph.D. Student, School of Civil Engineering, Tianjin University, Tianjin 300072, China; Staff, Airport College, Civil Aviation University of China, Tianjin 300300, China (Corresponding Author, E-mail: 549841779@qq.com)
**Professor, School of Civil Engineering, Tianjin University, Tianjin 300072, China (E-mail: tdwjh@tju.edu.cn)
***Professor, Airport College, Civil Aviation University of China, Tianjin 300300, China (E-mail: cauczxm@126.com)
****Associate Professor, Dept. Civil and Environmental Engineering, Rutgers University, Piscataway 08854, USA (E-mail: hwang.cee@rutgers.edu)
*****M.Sc. Student, Airport College, Civil Aviation University of China, Tianjin, Tianjin 300300, China (E-mail: 572565303@qq.com)

the taxiway width to which it connects. It must meet the requirements of the widest aircraft that will taxi across it, while its span should be no more than 20 m in consideration of economic factors. Hence, the width–span ratio of a taxiway bridge can be in the range 3 – 4, and that is much larger than that of typical highway bridge (usually less than 1). This results in the mechanical behavior of a taxiway bridge being different from that of a highway bridge.

As discussed above, the method for assessing the bearing capacity of highway bridge is not appropriate for taxiway bridge. In this paper, a new method which updates the initial finite element model (FEM) using frequency and strain influence lines measured in the field was proposed to evaluate a taxiway bridge accurately and efficiently and the existing disadvantages are overcome.

As modal parameters are sensitive to structural strength (Ragland *et al*., 2011; Panetsos *et al*., 2010), in highway bridges, FEM updating is roughly implemented by dynamic modal parameter (Zhou *et al.*, 2018; Esfandiari *et al.*, 2016; Zhou *et al*., 2015; Garcia-Palencia *et al.*, 2015; Caglayan *et al*., 2014; Meruane, 2011; Esfandiari *et al*., 2009). Some experts have also committed to the study of FEM updating by static parameters only (Lu, 2017; Yuan, 2016; Feng *et al*., 2015; Cardini, 2009). Both methods mentioned above have their disadvantages. On the one hand, the dynamic parameter measured in field is easy to fluctuate with environmental changes and the modal parameters are insensitive to structural damage. On the other hand, static test in field is time consuming and the traffic must be interrupted. So pseudo static method is adopted in this paper. The FEM is updated by frequency and strain influence lines. In highway bridges, some experts have started to conduct research in this area (Wang, 2018; Xiao *et al*., 2015; Bakhtiari-Nejad, 2005), but it is rare to see in taxiway bridges.

2. Analysis Methodology

2.1 Combination of FEM and Field Measurements

The proposed virtual load rating method is based on FE (finite element) model updating in terms of vibration frequency, strain, and deflection influence lines. The flowchart of model updating processes and virtual load rating method are illustrated in Fig. 1. Acceleration, strain, and inclinometer sensors were installed at appropriate positions under the bridge, clear of the aircraft's suspension. Then, the acquisition systems were used to collect the vibrational acceleration, structural strain and inclinometers when an aircraft taxis across the bridge. There are more than enough flights at large, busy airports to allow the actual structural responses under various aircraft with different loads to be collected over a relatively short time. Totally 10 groups of data under 10 aircraft of no fewer than five different types are collected. At the same time, the initial FEM of the taxiway bridge was established using ANSYS according to design and construction data. Because of discrepancies during construction and bridge condition deterioration during service, the initial FEM is unlikely to reflect the current state of the bridge. The FEM was required to be updated on the basis of multiple modal and strain influence lines measured in the field (10 groups of data). Parameters obtained from every group may be different, the weighted average algorithm calculated by weight of aircraft was used to ensure that the actual FEM is acquired. Ultimately, different loads are applied to the FEM to analyze the carrying capacity of the bridge.

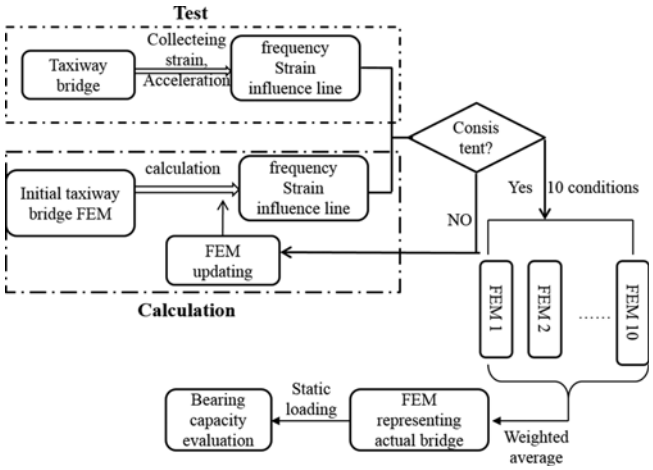

Fig. 1. Flow Chart of FE Model Updating and Virtual Load Rating Method

The following three key issues must be addressed in the testing process.

2.2 Dynamic Aircraft Load

The finite element analysis would be more accurate if the dynamic aircraft load imposed on bridge deck could be determined accurately. The force imposed on the bridge by an aircraft is influenced by the roughness of deck pavement and the wing lift generated as the aircraft taxis across the bridge. The latter component depends on the taxiing speed. As the aircraft speed increases, the dynamic load caused by pavement roughness increases accordingly. However, the increasing taxiing speed also increases the lift force produced by the aircraft wings. Hence, it reduces dynamic aircraft load applied on bridge deck. Therefore, the dynamic aircraft load is a function of taxiing speed.

Previous studies focused mainly on dynamic loading of vehicles travelling on highways or bridges (Zhu *et al.*, 2018; Yin *et al*., 2018; Zhou *et al.*, 2018). With the development of FE method, some researches have studies aircraft–pavement interaction. Xu (1994) analyzed dynamic responses of rigid pavement under aircraft loading on the elastic half space. Zhang (Zhang and Sun, 2011) analyzed dynamic aircraft loads using a coupled aircraft–pavement system. The relationship between dynamic load coefficient and roughness, speed is researched. However, these studies were implemented from the perspective of coupling analysis, but failed to establish a relationship between dynamic load and International Roughness Index (IRI).

In highway engineering, Huang and Sheng (2006) used the power spectral density of pavement surface profile to obtain the mathematical relationship between dynamic load coefficient K and the IRI using a quarter car model:

$$K = 1 + 11.5c_0 \mathrm{IRI}\sqrt{v} \tag{1}$$

where coefficient $c_0 = 10^{-3}$ m$^{-0.5}$s$^{0.5}$, v [m/s] is the vehicle speed, K is dynamic load coefficient, and IRI is International Roughness Index.

According to conventional flight dynamics (Fang, 2005), the lift force Y produced by the aircraft wings as the aircraft taxis on the deck can be calculated using Eq. (2):

$$Y = \frac{1}{2}\rho v^2 C_y S \tag{2}$$

where ρ [kg/m^3] is the air density, s [m^2] is the wing area, C_y is the lift coefficient, and v [m/s] is the taxiing speed.

Hence, the vertical pavement load P_v of taxiing aircraft can be expressed using Eq. (3):

$$P_v = m_2 g(1 + 11.5c_0 \mathrm{IRI}\sqrt{v}) - Y \tag{3}$$

where m_2 [kg] is the mass of the aircraft, Y [kN] is the lift, v [m/s] is the taxiing speed, and $c_0 = 10^{-3}$ m$^{-0.5}$s$^{0.5}$

Once the aircraft has accelerated to its takeoff speed, the load imposed on the pavement is zero. At that instant, Eq. (4) is stratified:

$$m_2 g(1 + 11.5c_0 \mathrm{IRI}\sqrt{v_0}) = Y \tag{4}$$

Equation (5) can be obtained by substituting Eq. (2) into Eq. (4):

$$m_2 g = \frac{\frac{1}{2}\rho v_0^2 C_y S}{1 + 11.5c_0 \mathrm{IRI}\sqrt{v_0}} \tag{5}$$

where v_0 [m/s] is the liftoff speed, ρ [kg/m^3] is the air density, s [m^2] is the wing area, C_y is the lift coefficient, m_2 [kg] is the mass of the aircraft and $c_0 = 10^{-3}$ m$^{-0.5}$s$^{0.5}$.

If K' is used to represent the dynamic load coefficient, Eq. (6) can be obtained from Eqs. (1) – (5).

$$K' = 1 + 11.5c_0 \mathrm{IRI}\sqrt{v} - \frac{1 + 11.5c_0 \mathrm{IRI}\sqrt{v_0}}{v_0^2} v^2 \tag{6}$$

where K' is the dynamic load coefficient, v_0 [m/s] is the liftoff speed, $c_0 = 10^{-3}$ m$^{-0.5}$s$^{0.5}$, v [m/s] is the taxiing speed, and IRI is International Roughness Index.

Hence, the dynamic aircraft load is show in Eq. (7):

$$F = K'G \tag{7}$$

where F [kN] is the dynamic aircraft load, and G [kN] is the static aircraft load.

The evaluation criteria of roughness are divided into three levels by the IRI average, according to the "Technical specifications of aerodrome pavement evaluation and management" (MH/T 5004-2009, 2009). These are listed in Table 1.

Table 1. Roughness Evaluation Criteria

Grade	Good	Medium	Poor
IRI average	< 2.0	2.0 – 4.0	> 4.0

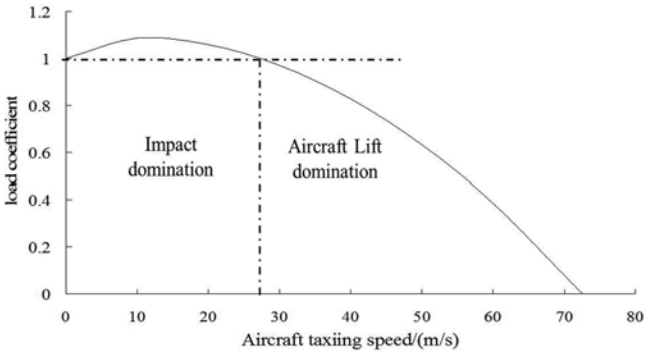

Fig. 2. Dynamic Load Coefficient Curve of a Boeing 737-800

The dynamic load coefficient curve of Boeing 737–800 is shown in Fig. 2 for a particular roughness. The results show that the dynamic load coefficient changes with taxiing speed. At rest, the dynamic load coefficient is one, i.e., the "dynamic" load is equal to the static load. As the aircraft begins taxiing, the dynamic load increases initially. However, at a critical taxiing speed, the increasing of lift force begins to dominate. The dynamic load coefficient decreases, thereafter, becoming zero at liftoff speed, i.e., the aircraft tire is no longer in contact with the runway pavement. Hence, it is concluded that pavement roughness dominates when the aircraft is taxiing slowly, whereas lift dominates for taxiing speeds of more than approximately 100 km/h (28 m/s).

In field tests, the taxiing speed can be calculated from the spacing between acceleration sensors and the time difference between corresponding acceleration peaks. Aircraft usually cross a taxiway bridge at a speed of 15 – 30 km/h (8 – 16 m/s), at which the impact of roughness is dominant.

2.3 Optimal Parameters and Objective Function for Model Updating

There has been considerable research on optimal parameters and objective function. For example, Friswell and Mottershead (1995) considered different parameter selections in dynamic FEM updating and analyzed their sensitivity. Feng and Feng (2015) analyzed the influence of traveling speed on FEM updating. Jang (2017) conducted sensitivity analysis to precisely understand the effects of physical parameters in the FE model on natural frequencies.

Various field tests have shown that strains and deflections of bridges are more obvious than other mechanical responses, and can accurately reflect the local behavior at the observation point. In contrast, the bridge modal parameters reflect the overall performance of structure. Therefore, vibration frequency and strain influence lines were used for FEM updating in this study. This can compensate for the inadequacy of updating with dynamic or static data alone. The objective function is given as

shown in Eq. (8):

$$f(X) = \sum_{i=1}^{n} \left(\frac{f_a - f_t}{f_t}\right)^2 + \sum_{i=1}^{n} \left(\frac{\varepsilon_a - \varepsilon_t}{\varepsilon_t}\right)^2 \quad (8)$$

where X is a design variable, f_a is the fundamental vibration frequency calculated from the initial FEM, f_t is the fundamental vibration frequency obtained from field tests, ε_a is the strain at test spot calculated from the initial FEM, ε_t is the strain at test spot obtained from field tests, and i is the number of test spots.

2.4 Weighted Model Parameters

When the FEM is updated at different aircraft loading conditions, the model parameters obtained by each condition may be different. The heavier the aircraft is, the response of bridge is more obvious and the actual data is believed more accurate. Therefore, the weight coefficients were calculated based on dynamic loads of aircrafts. The weight coefficient of each loading condition was determined from the dynamic aircraft load. A heavier aircraft with complex landing gear was given a greater weight, whereas a lighter aircraft was assigned a smaller weight. The calculation method of weights is given in Eq. (9):

$$\alpha_i = \frac{m_i}{\sum_{i=1}^{n} m_i} \quad (9)$$

where α_i is the weight coefficient of each loading condition, and m_i [kN] is dynamic aircraft load of each condition. In addition,

$$\bar{x} = \sum_{i=1}^{n} \alpha_i x_i \quad (10)$$

where $\bar{x}$ is the weighted average of a parameter and x_i is the parameter obtained from each loading condition.

3. Field Testing

3.1 Data Collection

The BDI-STS-WIFI Structural Testing System (shown in Fig. 3) produced in the United States is used in the dynamic testing technology. It includes various sensors (acceleration, strain, and tilt), wireless data transmission nodes, wireless base stations, and a data collection terminal. The acceleration sensors are used to collect the structural vibration signal, from which the inherent frequency and mode shape can be obtained by modal acceleration analysis. The strain and tilt sensors are used to collect the structural strains and inclinations at the test sites under aircraft loading.

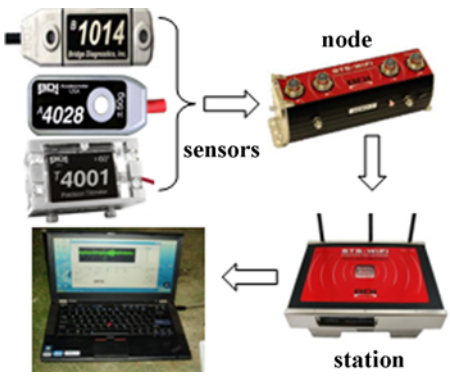

Fig. 3. Testing System

Fig. 4. Taxiway Bridge V

Taxiway Bridge V runs between the east and west airfields. Aircrafts are divided into different grades (A, B, C, D, E, and F) according to their structure and weight. The allowed loadings of Taxiway Bridge V is E. It is a pre-stressed cast-in-situ concrete beam bridge that has two 16-m-long spans. The width of the bridge is 65.5 m. The diameter of each pre-stressed, high-strength, low-relaxation steel strand is 15 mm. The bridge piers are thin-walled, bored piles. The beam is made from cast-in-situ pre-stressed concrete that has cube compressive-strength of 50 MPa. The bridge piers and abutments are made from cast-in-situ concrete having cube compressive-strength of 30 MPa. Taxiway Bridge V is shown in Fig. 4.

The sensors were attached on the underside of beam on the first span from the west. As shown in Fig. 5(a), acceleration sensors A2038, A2031, and A2067 were attached at quarter span, mid span, and three-quarters span so that the vibration mode could be obtained in the data-analysis stage. The strain sensors were arranged at two cross sections on the underside of deck: Quarter span (test line 1) and mid span (test line 2). The spaces between the sensors were shown in Fig. 5(b). The inclinometers were divided into three test lines. The separation between test lines was 6.25 m, as shown in Fig. 5(c). When an aircraft passed across the taxiway bridge, the sensors collect the vibration accelerations, strain influence lines, and inclinations at the measurement points. The site photos were as shown in Fig. 6.

3.2 Data Analysis

The dynamic responses were collected under 10 aircraft (six types) taxiing over the bridge. All the data showed the same trend, and differed only in the peak values and their occurring

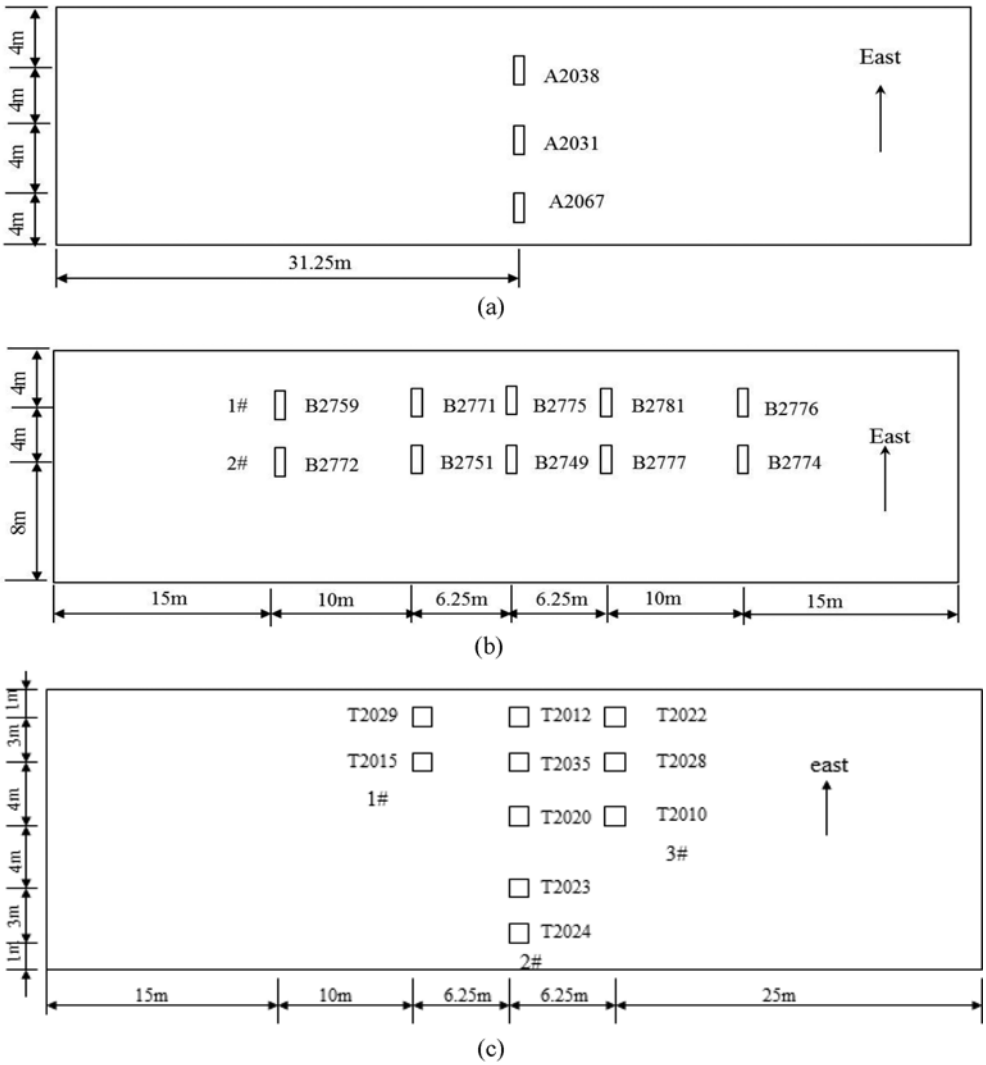

Fig. 5. Arrangement of Sensors: (a) Acceleration Sensors, (b) Strain Sensors, (c) Tilt Sensors

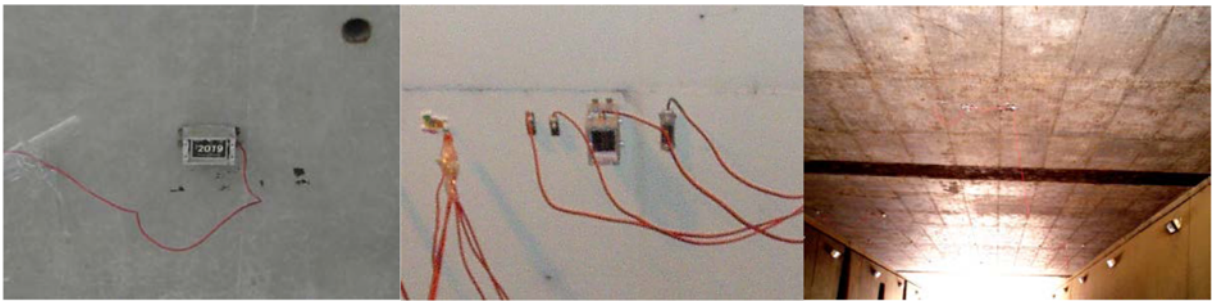

Fig. 6. Sensors on Taxiway Bridge V

times. Hence, only one group of data analysis results were presented as follows. The IRI of pavement on taxiway bridge V is 0.86. The taxiing speeds, static loads, and dynamic loads (calculated by dynamic load coefficient and static load) of the 10 aircraft were given in Table 2.

3.2.1 Acceleration Spectral Analysis: Fundamental Vibration Frequency

Accelerations collected by A2038 are shown in Fig. 7. The fundamental frequency of Taxiway Bridge V was found being 13.11 Hz after fast Fourier transform (FFT), as shown in Fig. 8.

3.2.2 Strain–Time History

The strain sensor at each point recorded the strain during the entire process from the aircraft first arriving on the bridge to

Table 2. Aircraft Loads under 10 Conditions

Aircraft	Taxiing speed (km/h)	Static load (kN)	Dynamic load (kN)
B738	18	782	795
B73G	16	645	660
B738	19	685	697
B773	18	2,800	2,848
A320	18	815	829
B738	15	712	729
B772	19	2,735	2,781
B787	20	1,651	1,676
B738	20	715	726
B738	19	725	736

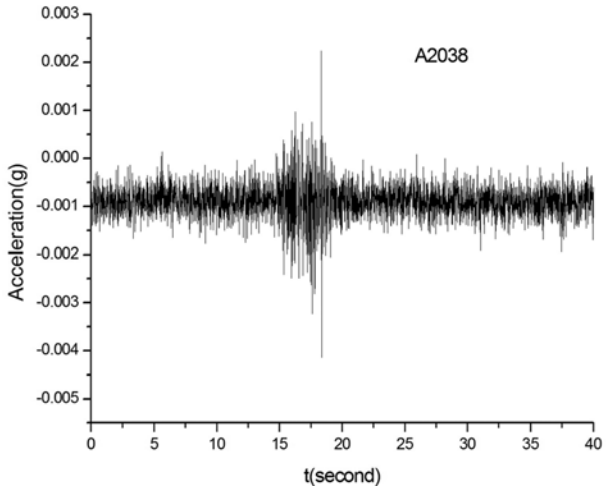

Fig. 7. Acceleration Signal Tested by A2038

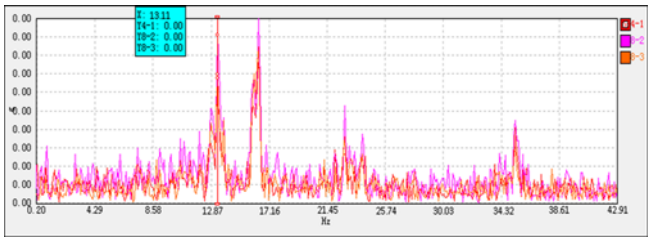

Fig. 8. Spectrum Analysis

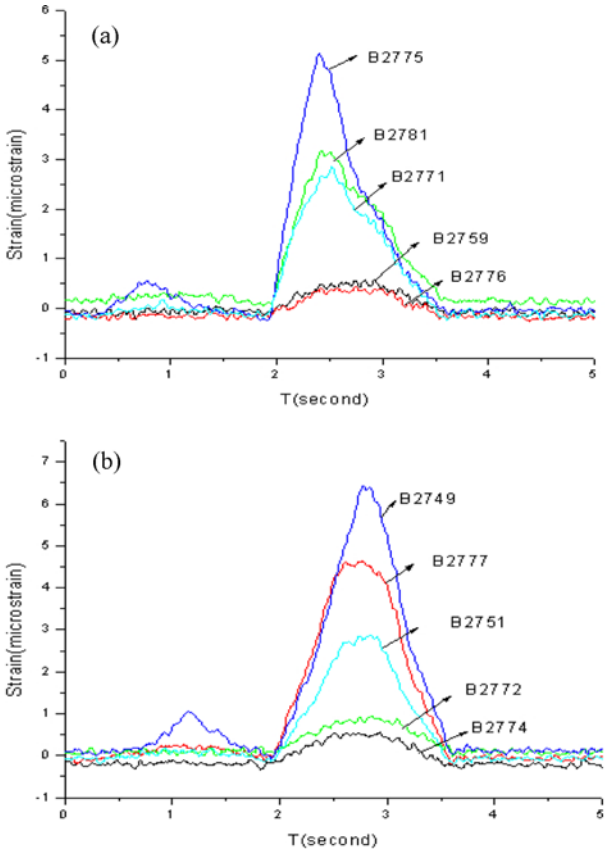

Fig. 9. Strain–Time Curves: (a) Test Line 1, (b) Test Line 2

completely leaving it. Fig. 9 shows the strain–time curve at test line 2 under A320 passing along the midline of the deck. The strain peaks were collected.

3.2.3 Inclinations

When the A320 aircraft passed across the deck along the midline, the inclination–time curves of each point was plotted in Fig. 10. The deflections of taxiway bridge can be calculated on the basis of the inclinations (Yang, 2010).

4. Model Updating Results

4.1 Initial FEM Results

Since Taxiway Bridge V was an integral cast-in-situ concrete structure, its transverse connection was in good condition and there were no apparent cracks at the beam surfaces. The initial FEM of Taxiway Bridge V could be established from its design drawings. A parametric modeling method was adopted (Gong, 2004). The dimensions of the cross section, pre-stress, elastic modulus, and other parameters were set as variables. Pre-stressed steels were simulated by Link8 and concrete was simulated by Solid65 in ANSYS. The prestressed steels were coupled with the surrounding concrete as a whole by the coupling equation, and the prestress was transmitted to the surrounding concrete by the cooling method. The FEM was given in Fig. 11.

It can be seen from the measured data that the taxiing speed of the A320 is 5.2 m/s. Combining with other parameters, the calculated dynamic load coefficient was 1.017. The dynamic aircraft load of the A320 was imposed on the deck along the midline to simulate the whole process of aircraft taxiing, and the strain at each point was calculated. The strain peaks were given in Table 3.

The strain errors of the measured and calculated values were shown in Table 4. It was found that the measured strains of many sites were not consistent with the calculated values, and that the strains of some sites even differed by more than 35%. Hence, the updating process of FEM was essential.

The calculated fundamental frequency of the initial FEM was 13.98 Hz, which differed by 6.7% from the measured value in

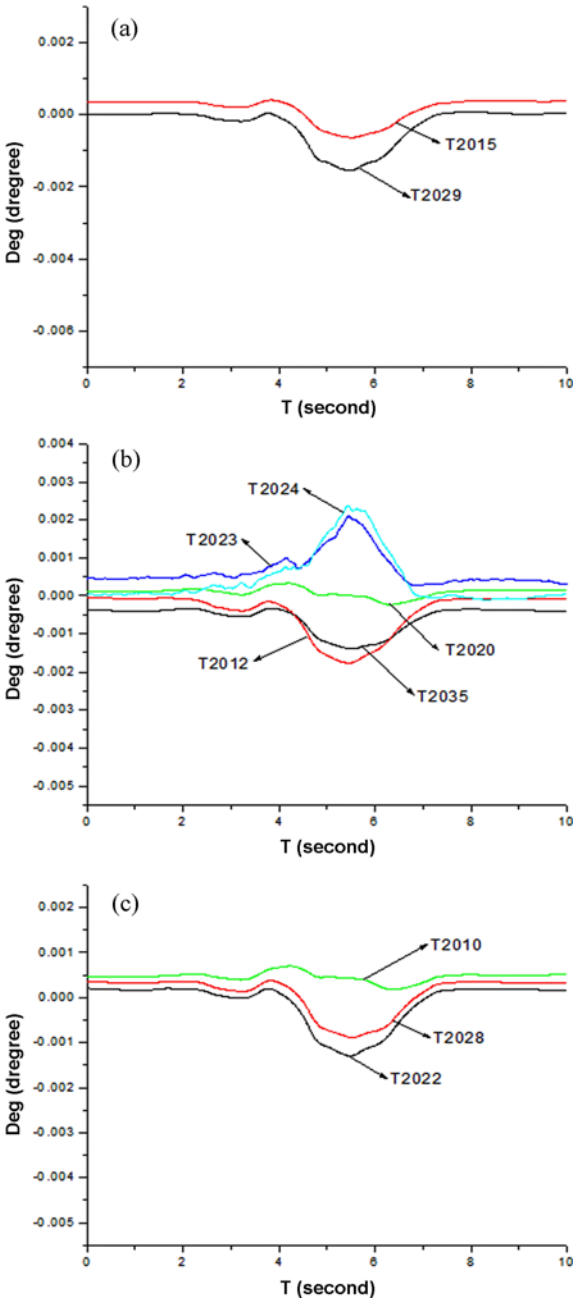

Fig. 10. Inclination–Time Curves: (a) Test Line 1, (b) Test Line 2, (c) Test Line 3

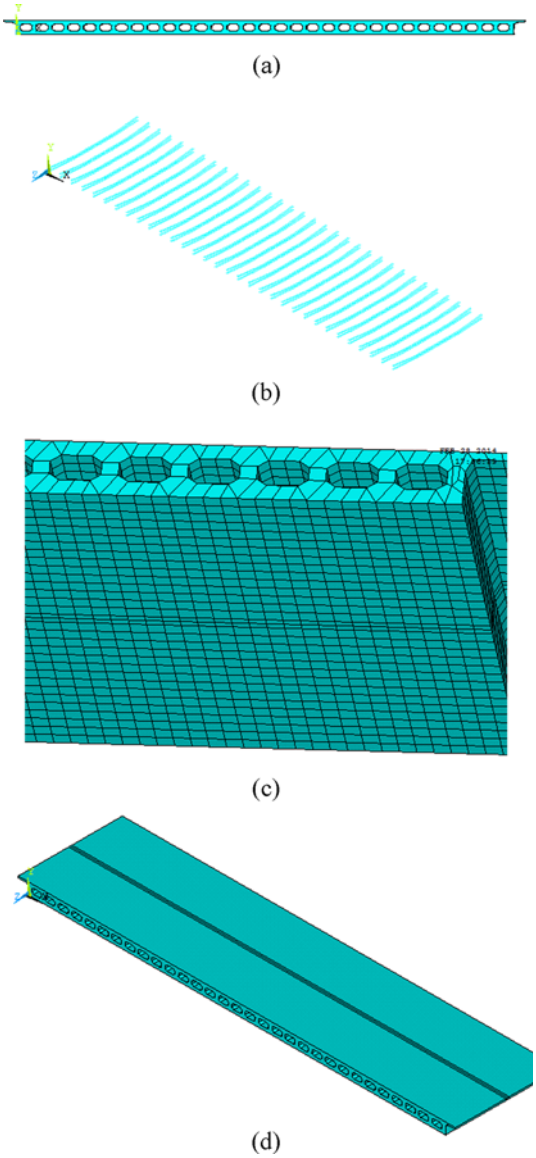

Fig. 11. Initial FEM: (a) Cross Section, (b) Pre-stressed Reinforcement, (c) Mesh, (d) FEM

Table 3. Calculated Strain Peaks under Aircraft A320

Test line 1		Test line 2	
Sensor	Peak value ($\mu\varepsilon$)	Sensor	Peak value ($\mu\varepsilon$)
B2775	4.98	B2749	6.42
B2771	4.16	B2777	5.87
B2781	2.84	B2751	4.01
B2759	1.18	B2772	1.29
B2776	0.98	B2774	1.05

the field, as shown in Table 5.

4.2 FEM Results after Updating

In the process of FEM updating, the frequency and strain peak at each site under the B738 provided the main basis for optimization; other measured strains play secondary roles. The calculated fundamental frequency and strains should be in more than 90% agreement with the test values after the iterative calculation process.

The design variables were the pore sizes of the hollow plate shown in Fig. 12, represented by a (m) and b (m), the thickness of bridge deck, represented by t (m), the elastic modulus of main beam, represented by E_1 (MPa), the elastic modulus of the deck pavement, represented by E_2 (MPa), the height of the main beam, represented by h (m), and the volume weight, represented by γ (KN/m^3). The bridge pavement was steel-fiber-reinforced concrete having cube compressive-strength of 50 MPa. Since steel fiber

Table 4. Error of Strains

Test line	Sensor	Calculated value ($\mu\varepsilon$)	Measured value ($\mu\varepsilon$)	Error
1	B2775	4.98	4.30	13.6%
	B2771	4.16	3.89	6.5%
	B2781	2.84	2.71	4.6%
	B2759	1.18	0.95	19.5%
	B2776	0.98	0.87	11.2%
2	B2749	6.42	6.28	2.2%
	B2777	5.87	5.49	6.5%
	B2751	4.01	4.33	-8.0%
	B2772	1.29	1.14	11.6%
	B2774	1.05	0.67	36.2%

Table 5. Error of Fundamental Frequency

Frequency	Calculated value (Hz)	Measured value (Hz)	Error
First-order	13.98	13.11	6.7%

plays an important role in increasing the elastic modulus and strength of concrete, the initial elastic modulus of pavement was $E_2 = 4.00 \times 10^4$ MPa. The initial values of design variables were as follows:

$a = 0.9$ m

$b = 0.4$ m

$E_1 = 3.35 \times 10^4$ MPa

$E_2 = 4.00 \times 10^4$ MPa

$t = 0.15$ m

$h = 1.7$ m

$\gamma = 25\text{KN/m}^3$

Taking construction and design variation into account, the reasonable ranges of design variables were limited as follows:

$0.6\text{ m} \le a \le 1.1\text{ m}$

$0.2\text{ m} \le b \le 0.6\text{ m}$

$3.25 \times 10^4\text{ MPa} \le E_1 \le 3.75 \times 10^4\text{ MPa}$

$3.75 \times 10^4\text{ MPa} \le E_2 \le 4.25 \times 10^4\text{ MPa}$

$0.10\text{ m} \le t \le 0.20\text{ m}$

$1.6\text{ m} \le h \le 1.8\text{ m}$

$24\text{ KN/m}^3 \le \gamma \le 27\text{ KN/m}^3$

The objective function was:

$$f(a,b,E_1,E_2,t,h) = \sum_{i=1}^{n}\left(\frac{f_a - f_t}{f_t}\right)^2 + \sum_{i=1}^{n}\left(\frac{\varepsilon_a - \varepsilon_t}{\varepsilon_t}\right)^2 \quad (11)$$

The optimization module in ANSYS was used for the model iteration with the design variables and objective function. The strain errors were given in Table 6, and the frequency error was given in Table 7 after optimization. The first-order vibrational shape diagram was shown in Fig. 13.

Tables 6 and 7 showed that the calculated values were consistent with the measured values with a goodness of fit of

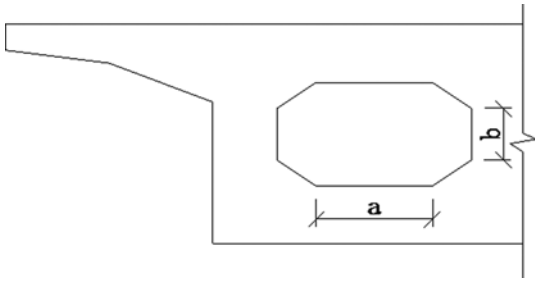

Fig. 12. Variables of Cross Section

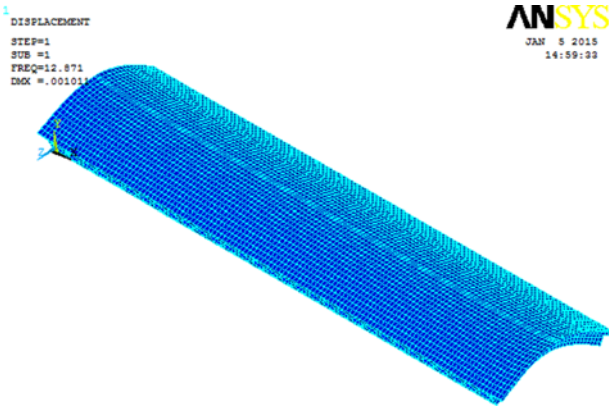

Fig. 13. First-Order Vibration Shape

Table 6. Error of Strains after Updating

Test line	Sensor	Calculated value ($\mu\varepsilon$)	Measured value ($\mu\varepsilon$)	Error
1	B2775	4.16	4.30	-3.4%
	B2771	3.98	3.89	2.3%
	B2781	2.82	2.71	3.9%
	B2759	0.97	0.95	2.1%
	B2776	0.95	0.87	8.4%
2	B2749	5.71	6.28	-9.9%
	B2777	5.47	5.49	-0.4%
	B2751	3.98	4.33	-8.8%
	B2772	1.06	1.14	-7.5%
	B2774	0.73	0.67	8.2%

Table 7. Error of Frequency after Updating

Frequency	Calculated value (Hz)	Measured value (Hz)	Error
First-order	13.52	13.11	3.1%

90%. Hence, the FEM updating can be considered successful. The strain influence lines before and after updating of the measuring points where B2775 and B2751 were pasted on are shown in Fig. 14. The similar updating process was repeated for the other FEM models under loading of different aircrafts. The 10 updated models had slightly different parameters. A weighting coefficient of each condition was assigned to the corresponding parameter group. Hence, the FEM representing the actual status of Taxiway Bridge V was obtained.

The remaining nine FEM updating were repeated, and 10

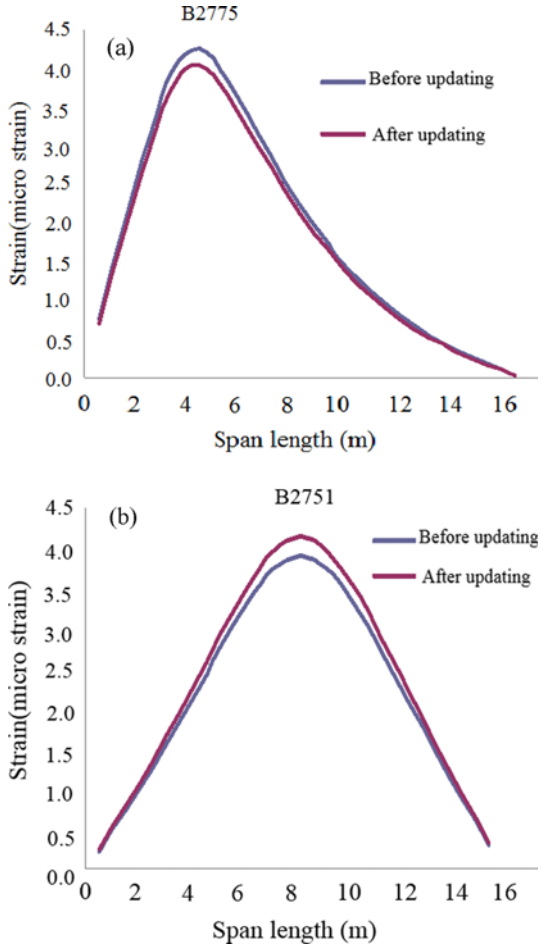

Fig. 14. Updating by Strain Influence Line: (a) B2775, (b) B2751

FEMs with slightly different parameters were obtained. The weighting coefficient of each condition were calculated and they were assigned to the corresponding parameter group. The FEM representing the actual status of Taxiway Bridge V was obtained.

4.3 Accuracy Verification

To verify the accuracy of the optimized FEM, static loading test was conducted at the mid-span of the bridge. The aircraft was stationary for 2 min, during which static strains and deflections were collected. It was found that both the average error of strains at each site and the average error of deflections were less than 5% by comparing the measured values with those calculated by the updated FEM. This shows that the FEM can represent the true state of Taxiway Bridge V. Error analysis of FEM under B737 was shown in Table 8.

Table 8. Error Analysis of FEM under B737

Strain	Midspan	Deflection	Midspan
Calculated strain ($\mu\varepsilon$)	11.3	calculated deflection (mm)	0.297
Tested strain ($\mu\varepsilon$)-B2749	11.8	Tested deflection (mm)-T2020	0.31
Error	-4.42%	Error	-4.38%

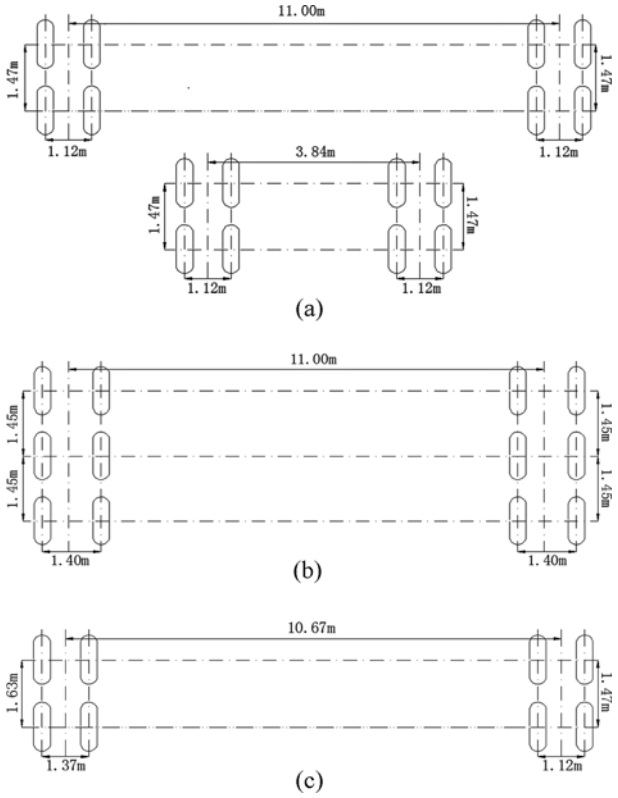

Fig. 15. Main Landing Gears: (a) B-747, (b) B-777, (c) MD-11

5. Virtual Load Rating

Design loads (Boeing 747 was used as the calculation load, Boeing 777 and MD-11 were used as check loads, main landing gears were shown in Fig. 15) were applied to the optimized FEM and deformations of Taxiway Bridge V were calculated. The equivalent deflection curves of Taxiway Bridge V under these three aircraft were shown in Figs. 16(a), 16(b), and 16(c). The strain calibration coefficients and deflection calibration coefficients were given in Table 9.

The results above show that the strain calibration coefficients and deflection calibration coefficients of Taxiway Bridge V were all less than 1 under the design loads, meeting loading efficiency. This indicated that the bridge meets the requirements of design specifications. However, since the calibration coefficients were close to 1, the long-term behavior of bridge should be monitored.

6. Conclusions

A new in situ test method using the updated FEM model for load rating of taxiway bridges is proposed. The field test can be carried out as at aircraft taxiing. The following findings can be concluded from the analysis:

1. The implementation process and procedures of the new test

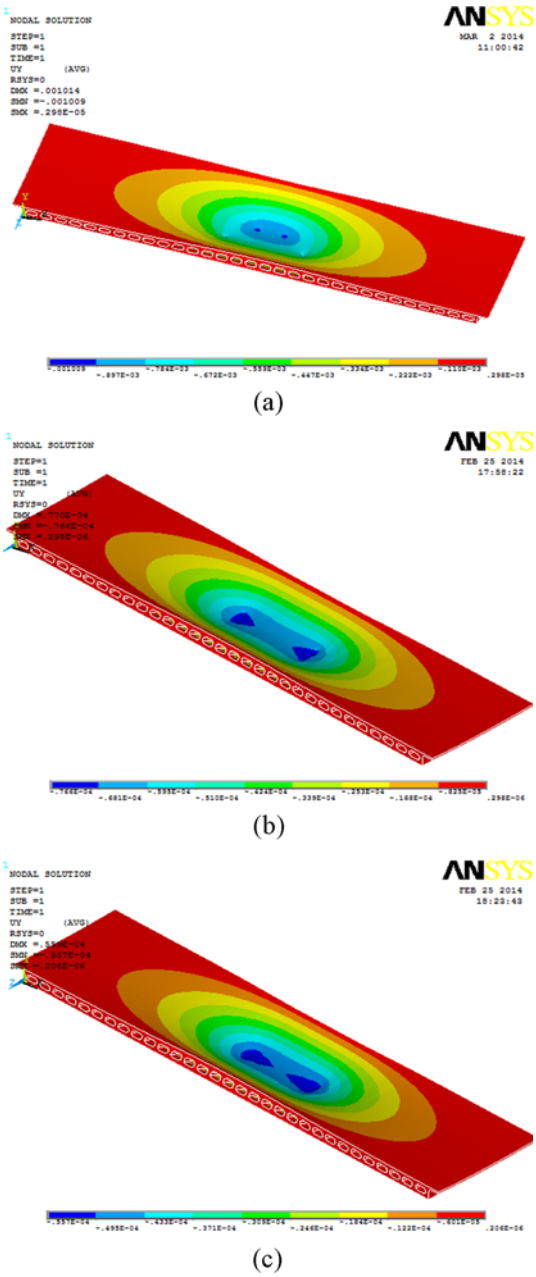

Fig. 16. Equivalent Deflection Curves of Taxiway Bridge V: (a) B-747, (b) B-777, (c) MD-11

Table 9. Strain Calibration and Deflection Calibration Coefficients

Taxiway Bridge V	B-747	B-777	MD-11
Designed strain ($\mu\varepsilon$)	33.9	29.0	18.4
Tested strain ($\mu\varepsilon$)	32.2	27.3	17.3
Calibration coefficient	0.95	0.94	0.94
Designed deflection (mm)	0.89	0.71	0.51
Tested deflection (mm)	0.85	0.68	0.49
Calibration coefficient	0.96	0.96	0.97

method are introduced, and their effectiveness and feasibility are demonstrated.

2. A dynamic aircraft load coefficient model is established, which takes the aircraft lift into consideration. The dynamic aircraft load increases at first, and then decreases with further increase in taxiing speed. It is concluded that pavement roughness dominates when the aircraft is taxiing slowly, whereas lift dominates for taxiing speeds of more than approximately 100 km/h (28 m/s).
3. The vibration mode and strain influence line measured in the field are both used for FEM updating in the bearing-capacity evaluation process of the taxiway bridge until the FEM representing the actual situation is obtained. This overcomes the drawbacks of updating with dynamic or static data alone. In the field test, it showed that the calculated values were consistent with the measured values with a goodness of fit of 90% after FEM updating.
4. A weighted average algorithm is proposed for updating process of FEM at different aircraft loading conditions to ensure the reliability of model updating.
5. The new test method is applied to four taxiway bridges at Guangzhou Baiyun International Airport (CAN) to evaluate their bearing capacities, and good results were achieved. It was found that both the average error of strains at each site and the average error of deflections were less than 5% by comparing the measured values with those calculated by the updated FEM.

References

Bakhtiari-Nejad, F., Rahai, A., and Esfandiari, A. (2005). "A structural damage detection method using static noisy data." *Journal of Structural Engineering,* ASCE, Vol. 27, No. 12, pp. 1784-1793, DOI: 10.1016/j.engstruct.2005.04.019.

Caglayan, O., Tezer, O., Ozakgul, K., and Piroglu, F. (2014). "In-situ field measurements and numerical model identification of a multi-span steel railway bridge." *Journal of Testing and Evaluation*, Vol. 43, No. 6, DOI: 10.1520/JTE20140049.

Cardini, A. J. and DeWolf, J. T. (2009). "Long-term structural health monitoring of a multi-girder steel composite bridge using strain data." *Structural Health Monitoring*, Vol. 8, No. 1, pp. 47-58, DOI: 10.1177/1475921708094789.

Esfandiari, A., Bakhthiari-Nejad, F., Rahai, A., and Sanayei, M. (2009). "Structural model updating using frequency response function and quasi-linear sensitivity equation." *Journal of Sound and Vibration*, Vol. 331, No. 8, pp. 1961-1961, DOI: 10.1016/j.jsv.2011.11.008.

Esfandiari, A., Rahai, A., Sanayei, M., and Bakhtiari-Nejad, F. (2016). "Model updating of a concrete beam with extensive distributed damage using experimental frequency response function." *Journal of Bridge Engineering,* ASCE, Vol. 21, No. 4, DOI: 10.1061/(ASCE)BE.1943-5592.0000855.

Fang, Z. P. (2005). *Aircraft flight mechanics,* Beihang University Press, Beijing, China.

Feng, D. M. and Feng, M. Q. (2015). "Model updating of railway bridge using in situ dynamic displacement measurement under trainloads." *Journal of Bridge Engineering*, Vol. 20, No. 12, pp. 199-211, DOI: 10.1061/(ASCE)BE.1943-5592.0000765.

Friswell, M. I. and Mottershead, J. E. (1995). *Finite element model updating in structural dynamics*, Kluwer Academic Publisher, Dordrecht, Netherlands.

Garcia-Palencia, A. J., Santini-Bell, E., Sipple, J. D., and Sanayei, M. (2015). "Structural model updating of an in-service bridge using dynamic data." *Structural Control & Health Monitoring*, Vol. 22, No. 10, pp. 1265-1281, DOI: 10.1002/stc.1742.

Gong, S. G. (2004). *ANSYS operation commands and parameterized programming*, China Machine Press, Beijing, China.

Huang, L. K. and Sheng, C. H. (2006). "Relationship between vehicle dynamic amplification factor and pavement roughness." *Journal of Highway and Transportation Research and Development*, Vol. 23, No. 3, pp. 27-30.

Jang, J. and Smyth, A. W. (2017). "Model updating of a full-scale FE model with nonlinear constraint equations and sensitivity-based cluster analysis for updating parameters." *Mechanical Systems and Signal Processing*, Vol. 83, No. 3, pp. 337-355, DOI: 10.1016/j.ymssp.2016.06.018.

Lu, Z. R., Zhu, J. J., and Qu, Y. J. (2017). "Structural damage identification using incomplete static displacement measurement." *Structural Engineering and Mechanics*, Vol. 63, No. 2, pp. 251-257, DOI: 10.12989/sem.2017.63.2.251.

Malerba, P. G. and Comaita, G. (2011). "Twin runway integral bridges at milano malpensa airport, Italy." *Structural Engineering International*, Vol. 21, No. 2, pp. 206-209, DOI: 10.2749/101686611X12994961034499.

Meruane, V. and Heylen, W. (2011). "A hybrid real genetic algorithm to detect structural damage using modal properties." *Mechanical Systems and Signal Processing*, Vol. 25, No. 1, pp. 1559-1573, DOI: 10.1016/j.ymssp.2010.11.020.

MH/T 5001-2013 (2013). *Technical standards for airfield area of civil airports*, MH/T 5001-2013, Civil Aviation Administration of China, Beijing, China.

MH/T 5004-2009 (2009). *Technical specifications of aerodrome pavement evaluation and management*, MH/T 5004-2009, Civil Aviation Administration of China, Beijing, China.

Panetsos, P., Ntotsios, E., Papadimitriou, C., Papadioti, D. C., and Dakoulas, P. (2010). "Health monitoring of metsovo bridge using ambient vibrations." *Structural Health Monitoring*, pp. 1081-1088.

Ragland, W. S., Penumadu, D., and Williams, R. T. (2011). "Finite element modeling of a full-scale five-girder bridge for structural health monitoring." *Structural Health Monitoring*, Vol. 10, No. 5, pp. 449-465, DOI: 10.1177/1475921710379515.

Stephan, S., Frank, Z., Horst, A., and Holger, M. (2012). "The taxiway bridges of the new runway northwest at the airport Frankfurt/Main." *Beton-und Stahlbetonbau*, Vol. 107, No. 3, pp. 164-174, DOI: 10.1002/best.201100084.

Wang, L. B. and Jiang, P. W. (2016). "Research on the computational method of vibration impact coefficient for the long-span bridge and its application in engineering." *Journal of Vibroengineering*, Vol. 18, No. 1, pp. 394-407.

Xiao, X., Xu, Y. L., and Zhu, Q. (2015). "Multiscale modeling and model updating of a cable-stayed bridge. II: Model updating using modal frequencies and influence lines." *Journal of Bridge Engineering*, Vol. 20, No. 10, DOI: 10.1061/(ASCE)BE.1943-5592.0000723.

Xu, J. Y. (1994). "FEM analysis of the dynamic coupling system consists of aircraft, pavement and soil." *Computational Structural Mechanics and Applications,* Vol. 11, No. 1, pp. 77-84.

Xu, Y. L., Sun, B., and Zhu, Q. (2018). "Updating multiscale model of a long-span cable-stayed bridge." *Journal of Bridge Engineering*, ASCE, Vol. 23, No. 3, p. 04017148, DOI: 10.1061/(ASCE)BE.1943-5592.0001195.

Yang, X. S., Yan, W. M., Chen, Y. J., He, H. X., and Yu, Q. G. (2010). "Bridge deflections testing method based on using inclinometers." *China Civil Engineering Journal*, Vol. 43, No. 3, pp. 106-111.

Yin, X. F., Liu, Y., and Kong, B. (2016). "Vibration behaviors of a damaged bridge under moving vehicular loads." *Structural Engineering & Mechanics*, Vol. 58, No. 2, pp. 199-216, DOI: 10.12989/sem.2016.58.2.199.

Yin, X. F., Liu, Y., Song, G., and Mo, Y. L. (2018). "Suppression of bridge vibration induced by moving vehicles using pounding tuned mass dampers." *Journal of Bridge Engineering*, Vol. 23, No. 7, p. 04018047, DOI: 10.1061/(ASCE)BE.1943-5592.0001256.

Yuan, P. P., Wang, Z. C., Ren, W. X., and Yang, X. (2016). "Nonlinear joint model updating using static responses." *Advance in Mechanical Engineering*, Vol. 8, No. 12, p.1687814016682651, DOI: 10.1177/1687814016682651.

Zaman, M., Taheri, M. R., and Alvappillai, A. (1991). "Dynamic response of a thick plate on viscoelastic foundation to moving loads." *International Journal for Numerical & Analytical Methods in Geomechanics*, Vol. 15, No. 9, pp. 627-647.

Zhang, X. M. and Sun, L. L. (2011). "Research on dynamic load coefficient based on the airfield pavement roughness." *Applied Mechanics and Materials*, Vols. 97-98, pp. 386-390, DOI: 10.4028/www.scientific.net/AMM.97-98.386.

Zhou, Y. F. and Chen, S. R. (2018). "Full-response prediction of coupled long-span bridges and traffic systems under spatially varying seismic excitations." *Journal of Bridge Engineering*, Vol. 23, No. 6, p. 04018031, DOI: 10.1061/(ASCE)BE.1943-5592.0001226.

Zhou, X. Q., Xia, Y., and Weng, S. (2015). "L-1 regularization approach to structural damage detection using frequency data." *Structural Health Monitoring*, Vol. 14, No. 6, pp. 571-582, DOI: 10.1177/1475921715604386.

Zhou, Y., Zhang, J. K., Yi, W. J., Jiang, Y. Z., and Pan, Q. (2018). "Structural identification of a concrete-filled steel tubular arch bridge via ambient vibration test data." *Journal of Bridge Engineering*, ASCE, Vol. 22, No. 8, p. 04017049, DOI: 10.1061/(ASCE)BE.1943-5592.0001086.

Zhu, J. and Zhang, W. (2018). "Probabilistic fatigue damage assessment of coastal slender bridges under coupled dynamic loads." *Engineering Structures*, Vol. 166, pp. 274-285, DOI: 10.1016/j.engstruct.2018.03.073.